UAS Sense and Avoid Integrity and Continuity: Intruder Linear Accelerations and Analysis

Michael B. Jamoom,* Adriano Canolla,† and Boris Pervan‡
Illinois Institute of Technology, Chicago, IL, 60616, USA

Mathieu Joerger§
University of Arizona, Tucson, AZ, 85721, USA

This research aims at developing methods to meet safety targets for sense and avoid (SAA) sensors of Unmanned Aircraft Systems (UAS) through integrity and continuity risk evaluation. This paper builds upon previous work that considered a constant velocity aircraft encounter model with a 2D analysis. We refine this model by accounting for intruder aircraft accelerations due to pilot actions, such as changes in thrust. These methods can determine the acceptability of a sensor or set of sensors. A 3D sensitivity analysis of intruder trajectories evaluates the impact on integrity and continuity of sensor noise, range and sample interval. The methods described in this research can be used to set potential SAA sensor requirements for UAS integration into the National Airspace System.

I. Introduction

Within the last decade, unmanned aircraft systems (UAS) operations have rapidly expanded, encompassing a wide range of civil and commercial applications [1]. In response to these rapidly expanding UAS operations, the United States Congress mandated the Federal Aviation Administration (FAA), through the *FAA Modernization and Reform Act of 2012*, to develop requirements necessary for broader UAS access into the National Airspace System (NAS) [2]. The FAA must meet this mandate while simultaneously ensuring airspace safety. This requires a UAS "sense and avoid" (SAA) capability, which provides the UAS with the self-separation (SS) protection necessary to remain "well clear" of other aircraft. SAA is analogous to the "see and avoid" responsibility for pilots of manned aircraft [1].

For manned own aircraft, if an intruder aircraft is cooperative, that is, employing an operating transponder or Automatic Dependent Surveillance - Broadcast (ADS-B) [3], air traffic control (ATC) may provide separation or a Traffic Collision Avoidance System (TCAS) could help the pilot detect the intruder as an aid to SS. Otherwise, if the intruder aircraft is non-cooperative, without an operating transponder or ADS-B, the manned aircraft pilot will not have the help of ATC or TCAS. In this manned aircraft case, it is solely the pilot's responsibility to visually see the intruder and maneuver to maintain separation. Without a pilot on board, an unmanned air vehicle (UAV) must employ a sensor (or suite of multiple sensors) to replicate the functionality of pilot vision. Detection of non-cooperative aircraft will require, for example, an electro-optical (EO), infrared (IR) or radar sensor. This sensor must adequately provide

*Senior Research Associate, Department of Mechanical, Materials and Aerospace Engineering, 10 W 32nd Street, Room 243, Member AIAA.
†PhD Candidate, Department of Mechanical, Materials and Aerospace Engineering, 10 W 32nd Street, Room 243.
‡Professor, Department of Mechanical, Materials and Aerospace Engineering, 10 W 32nd Street, Room 243, Associate Fellow AIAA.
§Assistant Professor, Department of Aerospace and Mechanical Engineering, 1130 N. Mountain Ave., P.O. Box 210119, Senior Member AIAA.

intruder measurements to the UAS SAA system, which will use these measurements to estimate potential intruder tracks and then determine whether a separation maneuver is required.

The Second FAA SAA Workshop [4] concluded that the concept of "well clear" is an airborne separation standard, i.e. a pilot will apply self-separation (SS) to remain well clear from other aircraft. With "well clear" subjectively referenced in the right-of-way rules, 14 CFR 91.113 [5, 6], there have been numerous proposals for objective well clear thresholds (WCT) [7, 8]. The UAS Sense and Avoid Science and Research Panel (SARP), originally established in 2011 by the Office of the Under Secretary of Defense for Acquisition, Technology, and Logistics for Unmanned Warfare, recommended a WCT in 2014 [9]. This SARP recommendation informed RTCA Special Committee-228 (SC-228), which used the SARP WCT recommendation to define the term Detect and Avoid (DAA) Well Clear (DWC) in their Draft DAA Minimum Operational Performance Standards (MOPS) [10]. The DAA MOPS defines a loss of DWC as follows:

$$\text{Loss of DWC} = [0 \leq \tau_{mod} \leq \tau^*_{mod}] \cap [HMD \leq HMD^*] \cap [-h^* \leq d_h \leq h^*] \tag{1}$$

where the modified horizontal time to closest point of approach (τ_{mod}) has a threshold (τ^*_{mod}) of 35 seconds, the horizontal miss distance (HMD) has a threshold (HMD^*) of 4000 feet, and the current vertical separation (d_h) has a threshold (h^*) of 450 feet [10]. We will use these DWC thresholds as the WCT in our analysis.

Although the methodology outlined in this paper can be applied to small UAS (sUAS), this paper will focus on large UAS, which impact a larger portion of the NAS. Small UAS are defined as weighing less than 55 lbs [1, 2, 11], typically do not operate above 400 feet, and are governed by the recently approved 14 CFR 107 [11]. In this paper, the operating airspace will mirror those in the DAA MOPS, which addresses large UAS transitioning to and from 18,000 feet (Class A airspace), while traversing Class D, E, and G airspace in the NAS [10]. More specifically, this paper will focus on non-cooperative intruders, which are planned to operate primarily below 10,000 feet with speeds less than 250 knots indicated [12].

One way to ensure SAA safety is to meet predetermined targets, requiring methods to quantify safety performance as a function of sensor uncertainty. In prior work, the authors introduced methods to evaluate *integrity risk* and *continuity risk* as UAS SAA safety performance metrics [13, 14]. Integrity is a measure of trust that can be placed in the correctness of information supplied by the total system, including the ability to provide timely alerts when the system should not be used [15]. Continuity is the ability of the total system to perform its function without interruption during the intended operation [15]. These methods can be used to establish sensor performance requirements and can apply to any candidate sensor or sensor suite. In this paper, we refine this work by accounting for unknown intruder pilot thrust inputs in a 3D sensitivity analysis.

There have been several papers that provide overviews of the SAA problem [16, 17, 18, 19, 20]. Previous SAA work has tended to focus on mirroring safety studies applicable to the ubiquitous TCAS, applying risk ratios as safety

metrics [21, 22, 4, 23, 24, 25, 26, 27, 28, 29, 30, 31]. Our approach is different, focusing directly on the accepted aviation navigation certification standards that quantify integrity and continuity as safety factors [32]. Integrity and continuity are absolute measures of safety, not relative metrics, like risk ratios. This approach has been adopted by numerous navigation systems, such as the GPS Ground-Based Augmentation System (also known as Local Area Augmentation System (LAAS)) [15, 33, 34], the GPS Airborne-Based Augmentation System (ABAS) [35], and the GPS Satellite-Based Augmentation System (also known as Wide Area Augmentation System (WAAS)) [36, 37]. It is also the basis for the Navigation Integrity Category (NIC) concept in ADS-B [38, 39, 40]. For example, for LAAS, at near-zero visibility, navigation integrity requirements specify that no more than one undetected hazardous navigation system failure is allowed in a billion approaches [15]. Kelly and Davis broke down their proposed target level of safety for required navigation performance (RNP) into accuracy, integrity, and continuity requirements [41], which are three of the four parameters that quantify navigation system performance (the other being availability) [41, 42]. This research focuses on integrity and continuity because, due to the scale of the requirements, they are the most difficult requirements for avionics systems to achieve. For example, in aircraft approach navigation, integrity risk can have extremely stringent requirements on the order of one in a billion and continuity risk can have requirements on the order of one in a million [15]. In contrast, accuracy requirements are typically on the order of 95% [15].

Previous work developed methods to determine UAS SAA integrity and continuity risks based on a constant velocity model in 2D [13, 43]. A constant velocity model does not account for uncertainties in intruder aircraft dynamics. These uncertainties can be caused by wind gusts or intruder pilot actions, such as turns and accelerations of the intruder and own aircraft. This work focuses on uncertainties due to unknown intruder pilot changes in thrust. We implement a Kalman filter to account for these uncertainties [44]. Uncertainties due to wind gusts and intruder turns are left for future work.

The latest version of the draft DAA MOPS defines Hazard Zones and Non-Hazard Zones [10, 45]. Section 2.2.4.3.2. of the draft DAA MOPS describes these zones: “hazard and non-hazard zones are used to define the trade space for when alerts must and must not be generated, but are not meant to imply a specific implementation” [10]. This is slightly different than Kunzi, who defined these zones in his PhD thesis. He defines a hazard zone as where “if an aircraft penetrates this zone, the hazard is considered to be present, and therefore an alert should be issued” and he defines a Non-Hazard Zone as where “if an aircraft remains in this zone, no hazard is considered to be present and an alert is therefore undesirable” [46]. These zones are depicted in Figure 1.

The SAA system needs to alert to initiate SS maneuvers early enough to ensure the intruder aircraft remains outside the WCT, or Hazard Zone. The system also needs to avoid early alerts (EA) in the Non-Hazard Zone, which can also be referred to as a Self-Separation Threshold (SST) [47, 4]. The alert zone in between the Hazard Zone and the Non-Hazard Zone can also be referred to as a Self-Separation Volume (SSV) [47, 4] or a May Alert Zone [46].

This work accounts for uncertainties due to unknown intruder linear accelerations to develop expressions for integrity risk and continuity risk. Integrity risk is quantified as the probability that the system provides Hazardously

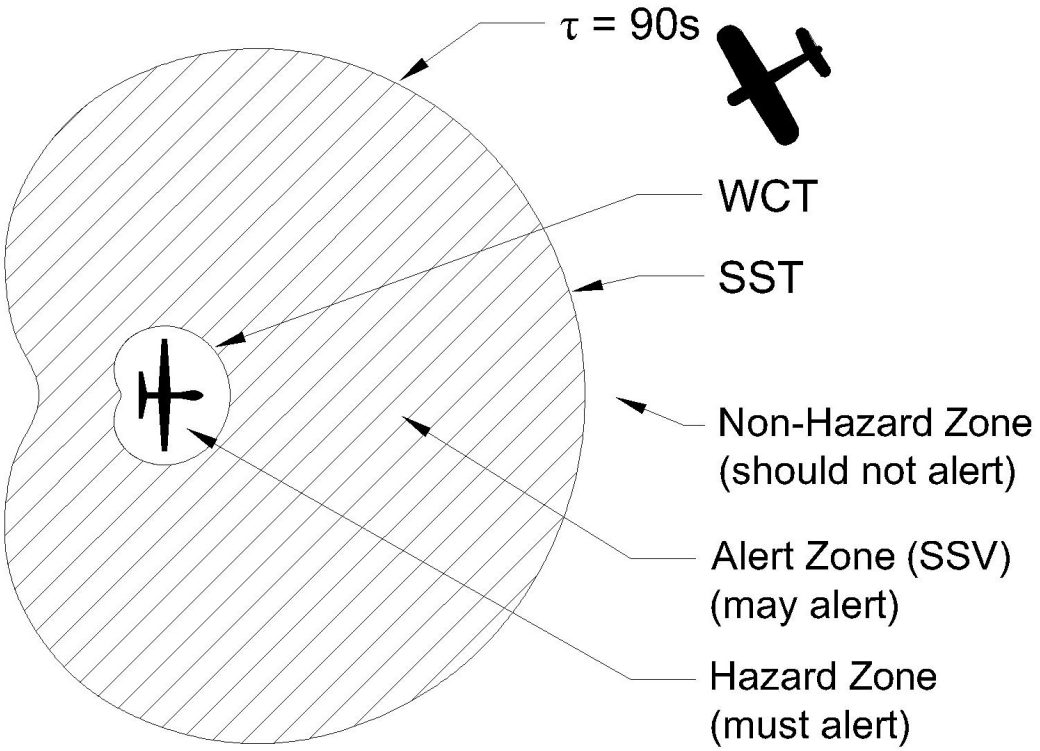

Figure 1. Hazard Zone and Non-Hazard Zone

Misleading Information (HMI) [48, 49], which is an unacceptably large error without a timely warning that the system cannot be trusted [42]. For the SAA problem, HMI occurs when the SAA system is not sensing a hazard (and not alerting to maneuver) but in fact, a hazard is present and a self-separation maneuver is required. This is analogous to the sum of missed alert and late alert described in [46]. Enge states that continuity fails when an aircraft operation is aborted for any unscheduled reason [49]. The major contributor to continuity risk is typically the probability of false alert [50, 51, 52, 49, 42]. For the SAA system, false alerts occur when alerts to maneuver are issued when no separation hazards are present. No separation hazards are present when alerts are early, prior to the Early Alert Threshold in the DAA MOPS (which corresponds to the temporal Non-Hazard Zone threshold) [10], or when alerts are nuisances, relating to intruder aircraft whose flight track remains in the Non-Hazard Zone [46]. For simplicity, we will measure continuity as the probability of early alert (EA), which for the purposes of this research, is the probability of an alert in either the temporal or spatial Non-Hazard Zones. A computationally efficient approach is introduced to determine bounds on the integrity risk and continuity risk. An example 3D sensitivity analysis examines the trade space between sensor performance, sample rates, integrity and continuity. The paper then shows how the new methods can be used to set potential SAA sensor requirements necessary for safe UAS-NAS integration.

After this introductory section, Section II introduces the 3D estimation model that accounts for uncertainty in intruder linear accelerations (based on uncertainty in intruder pilot thrust action) and estimates the hazard associated with a loss of well clear. Section III reviews the prior work methodology for implementing SAA integrity and continu-

ity. Section IV includes a 3D sensitivity analysis determining near-worst-case 3D trajectories and examining impacts of intruder pilot thrust inputs. Finally, Section V provides conclusions and opportunities for future research.

II. Relative Intruder State Estimation for Linear Accelerations

We present the SAA problem as a three dimensional, two-body problem. The two bodies are the own aircraft and the intruder aircraft. The coordinate frame is an own-aircraft-centered body frame. The details of this model, refined in the previous work [13], are outlined in the Appendix.

The trajectory state estimation model used to build the integrity and continuity risk methodology is based on a constant velocity assumption outlined in the DAA MOPS [10]. To refine this effort for constant accelerations, the trajectory state vector at time t_n, $\mathbf{x}_n$, now includes time variant intruder position and velocity, as well as constant acceleration:

$$\mathbf{x}_n = \begin{bmatrix} d_{x_n} & d_{y_n} & d_{h_n} & v_{x_n} & v_{y_n} & v_{h_n} & a_x & a_y & a_h \end{bmatrix}^T \tag{2}$$

Cartesian intruder position at t_n is denoted by $\begin{bmatrix} d_{x_n} & d_{y_n} & d_{h_n} \end{bmatrix}^T$, where d_{h_n} is the relative intruder altitude (or height) above the own aircraft. Cartesian intruder velocity is denoted by $\begin{bmatrix} v_{x_n} & v_{y_n} & v_{h_n} \end{bmatrix}^T$ and Cartesian constant intruder acceleration is denoted by $\begin{bmatrix} a_x & a_y & a_h \end{bmatrix}^T$.

The discrete-time process-noise-free state-transition equation is:

$$\mathbf{x}_n = \mathbf{F}\mathbf{x}_{(n-1)} \tag{3}$$

Where the constant state-transition matrix, $\mathbf{F}$, is:

$$\mathbf{F} = \begin{bmatrix} \mathbf{I}_{3\times3} & \Delta t\mathbf{I}_{3\times3} & \frac{\Delta t^2}{2}\mathbf{I}_{3\times3} \\ \mathbf{0}_{3\times3} & \mathbf{I}_{3\times3} & \Delta t\mathbf{I}_{3\times3} \\ \mathbf{0}_{3\times3} & \mathbf{0}_{3\times3} & \mathbf{I}_{3\times3} \end{bmatrix} \tag{4}$$

where $\mathbf{I}_{3\times3}$ is a 3 by 3 identity matrix, $\mathbf{0}_{3\times3}$ is a 3 by 3 matrix of zeros, and Δt is the sample rate.

The distribution of the error between the initial state, $\mathbf{x}_0$, and the initial state estimate, $\hat{\mathbf{x}}_0$, is:

$$\mathbf{x}_0 - \hat{\mathbf{x}}_0 \sim N\left(\left[\begin{array}{c} \mathbf{0}_{6\times1} \\ \hline \mathbf{0}_{3\times1} \end{array}\right], \left[\begin{array}{c|c} \bar{\mathbf{P}}_0 & \mathbf{0}_{6\times3} \\ \hline \mathbf{0}_{3\times6} & \mathbf{\Sigma}_a \end{array}\right]\right) \tag{5}$$

where $\bar{\mathbf{P}}_0$ is the initial position and velocity estimate error covariance (no prior knowledge is assumed on these states), and $\mathbf{\Sigma}_a$ is based on an expected distribution of pilot action. For example, a maximum 3-σ intruder acceleration of 1 knot/s can be derived from the intruder aircraft behavior distribution of the MIT Lincoln Lab Uncorrelated Encounter Model for the NAS [10, 53, 54].

In this work we only consider changes in the magnitude of the intruder aircraft velocity vector, its direction being assumed constant. The standard deviation of the specific force of the pilot action is noted σ_a and is in the head-on direction of the intruder body frame. This is converted into the own aircraft frame using the following equation:

$$\mathbf{\Sigma}_a = \mathbf{B} \begin{bmatrix} \sigma_a^2 & 0 & 0 \\ 0 & 0 & 0 \\ 0 & 0 & 0 \end{bmatrix} \mathbf{B}^T \tag{6}$$

where $\mathbf{B}$ is the transformation matrix from the intruder body frame to the own body frame.

A Kalman filter is used to estimate trajectory states, based on measurements described in the Appendix, and their estimate error covariance matrix, $\hat{\mathbf{P}}_n$, at each epoch n.

A. Hazard States Assuming Constant Velocity

For clarity of explanation in building up the hazard state estimation process, this subsection first assumes a constant velocity vector, which is consistent with Appendices D and G of the draft DAA MOPS [10]. The next subsection will refine this model by re-introducing the acceleration terms. In the draft DAA MOPS, SC-228 expanded on the SARP WCT recommendation and adopted the term loss of Detect and Avoid Well Clear (DWC) to describe the hazard associated with a loss of self-separation [10]. More specifically, the DAA MOPS defines a loss of well clear (or loss of DWC) in equation (1). In this loss of DWC definition, modified tau (τ_{mod}) is the actual (or true) time to horizontal closest point of approach (CPA) with an added safety factor [55]. That safety factor, D_{mod}, is a distance modifier that provides protection in encounters with a low rate of closure [4]. A loss of well clear occurs when τ_{mod} is at or within the tau threshold (τ^*_{mod}) *and* the horizontal CPA (r_{CPA} or HMD) is at or within the horizontal miss distance threshold (HMD^*) *and* the current vertical separation (d_h) is at or within plus/minus the vertical separation threshold (h^*).

Figure 2 is a top-view depiction of the CPA. For a loss of DWC, there has to be a time n, when d_h has to be at or within the vertical miss distance, $\pm h^*$, while the r_{CPA} is at or within the required horizontal miss distance, HMD^*, and τ_{mod} is at or within the self-separation threshold, τ^*_{mod}. All must be true simultaneously. If only h^* is violated, the intruder could be co-altitude, but hundreds of miles away. Conversely, if only HMD^* is violated, the intruder could be directly above or below the own aircraft, but off altitude by several thousand feet.

The DAA MOPS also defines alerting thresholds for Preventive, Corrective, and Warning Alerts. In each case, alerts are specified using a set of must alert and must not alert requirements. This is based on a predicted loss of Detect and Avoid Well Clear (DWC) as defined in equation (1) [10]. The alerting requirements are based on Hazard Zones and the must not alert requirements are based on Non-Hazard Zones. The different Alerting Thresholds are presented in Table 1, which is directly from the DAA MOPS DAA Alert Summary Table 2-21 [10].

Since the warning alert is the most restrictive and matches the DWC thresholds, the hazard states will be defined

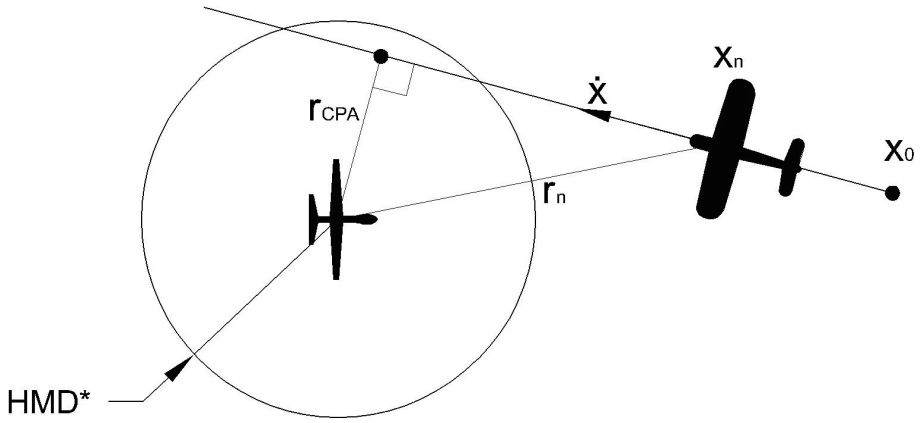

Figure 2. Overhead View of Closest Point of Approach

Table 1. DAA MOPS Alert Summary [10]

Alert Type	Hazard Zone				Non-Hazard Zone			
	Late Threshold	τ^*_{mod}	HMD^*	h^*	Early Threshold	τ^*_{mod}	HMD^*	h^* or V_{mod}
Preventive	20s	35s	0.66 NM	700 ft	75s	110s	2.0 NM	800 ft
Corrective	20s	35s	0.66 NM	450 ft	75s	110s	1.5 NM	450 ft
Warning	15s	35s	0.66 NM	450 ft	55s	90s	1.0 NM	450 ft

based on the predicted Warning Alert. Therefore, the hazard states are τ_{mod}, r_{CPA}, and h_p (the predicted intruder vertical position). The corresponding thresholds are τ^*_{mod} = 35 s, HMD^* = 4000 feet = 0.66 NM, and h^* = 450 feet [10]. The Late Alert time of 15 seconds will be used to define h_p.

For a loss of DWC hazard to exist, the following three events must simultaneously occur:

- The intruder trajectory horizontal CPA, r_{CPA}, must be within the HMD^*
- The intruder trajectory must vertically cross within $\pm h^*$ within 15 seconds
- τ_{mod} must be less than or equal to τ^*_{mod} within 15 seconds ($\tau_{mod} - 15s \leq \tau^*_{mod}$)

1. *Modified Horizontal Time to CPA*

Modified tau, τ_{mod}, is the actual (or true) time to horizontal closest point of approach with an added safety factor [55]. *True tau*, τ_{true}, is the actual time to horizontal closest point of approach assuming unaccelerated flight by both own aircraft and the intruder [55]. The DAA MOPS defines modified tau as follows for closing geometries [10]:

$$\tau_{mod} = \frac{-(r^2 - D^2_{mod})}{r\dot{r}} = \frac{D^2_{mod} - r^2}{d_x v_x + d_y v_y} \tag{7}$$

where r is the relative intruder horizontal range, $\dot{r}$ is the relative intruder horizontal range rate, d_x and d_y are the relative intruder Cartesian horizontal position distances and v_x and v_y are the relative intruder Cartesian horizontal

velocities.

D_{mod} is the distance modification, which is set equal to the horizontal miss distance threshold, HMD^*. If $D_{mod} \neq HMD^*$, the DAA MOPS explains that "alerts may oscillate on and off with un-accelerating ownship and intruder, which is an undesired behavior" [10].

Since $r = \sqrt{d_x^2 + d_y^2}$, modified tau can be defined completely as a function of the trajectory states:

$$\tau_{mod} = \frac{D_{mod}^2 - d_x^2 - d_y^2}{d_x v_x + d_y v_y} \tag{8}$$

2. Actual Time to Horizontal CPA

To get the Actual Time to Horizontal CPA, τ_{true}, in terms of trajectory states, the following two equations need to be solved:

$$\begin{bmatrix} d_{x_n} \\ d_{y_n} \end{bmatrix} + \tau_{true} \begin{bmatrix} v_x \\ v_y \end{bmatrix} = \begin{bmatrix} x_{CPA} \\ y_{CPA} \end{bmatrix} \tag{9}$$

$$\begin{bmatrix} v_x \\ v_y \end{bmatrix} \cdot \begin{bmatrix} x_{CPA} \\ y_{CPA} \end{bmatrix} = 0 \tag{10}$$

The first equation reflects the distance from the current horizontal position, $\begin{bmatrix} d_{x_n} & d_{y_n} \end{bmatrix}^T$, to the Cartesian horizontal CPA, $\begin{bmatrix} x_{CPA} & y_{CPA} \end{bmatrix}^T$, as a sum of position and τ_{true} times Cartesian horizontal velocity, $\begin{bmatrix} v_x & v_y \end{bmatrix}^T$. The second equation, which is the dot product of the horizontal Cartesian velocity vector and the horizontal Cartesian closest point of approach vector, expresses that these two vectors are perpendicular. Combining these equations results in three equations and three unknowns:

$$\begin{bmatrix} 1 & 0 & -v_x \\ 0 & 1 & -v_y \\ v_x & v_y & 0 \end{bmatrix} \begin{bmatrix} x_{CPA} \\ y_{CPA} \\ \tau_{true} \end{bmatrix} = \begin{bmatrix} d_{x_n} \\ d_{y_n} \\ 0 \end{bmatrix} \tag{11}$$

The resulting three unknowns, x_{CPA}, y_{CPA}, and τ_{true} can be computed using the following equations:

$$\begin{bmatrix} x_{CPA} \\ y_{CPA} \end{bmatrix} = \begin{bmatrix} d_{x_n} + \tau_{true} v_x \\ d_{y_n} + \tau_{true} v_y \end{bmatrix} \tag{12}$$

$$\tau_{true} = \frac{-(v_x d_{x_n} + v_y d_{y_n})}{v_x^2 + v_y^2} \tag{13}$$

3. *Horizontal Closest Point of Approach*

There are two ways to determine the Horizontal CPA, r_{CPA}. One is the-time based definition in the DAA MOPS and the other is geometrically determined based on a linear intruder trajectory. The time-based horizontal CPA from the DAA MOPS is [10]:

$$r_{CPA} = \sqrt{x_{CPA}^2 + y_{CPA}^2} = \sqrt{(d_{x_n} + \tau_{true} v_x)^2 + (d_{y_n} + \tau_{true} v_y)^2} \tag{14}$$

The geometric r_{CPA} is based on the intruder's linear trajectory. This expression for r_{CPA} is:

$$r_{CPA} = \sqrt{x_{CPA}^2 + y_{CPA}^2} = \frac{v_y d_x - v_x d_y}{\sqrt{v_x^2 + v_y^2}} \tag{15}$$

when factoring out τ_{true} in equation (14), equation (14) reduces to equation (15).

4. *Predicted Vertical Separation*

According to the DAA MOPS, the DAA system "shall provide a warning alert at least 15 seconds prior to an intruder entering the warning hazard zone" [10]. (This is 15 actual seconds, as computed using the true time to CPA, not 15 seconds as approximated using the τ_{mod} variable.) Therefore, there needs to be a predicted vertical separation, h_p, that can lookahead up to 15 seconds. This can be accounted for in the following equation:

$$h_p = d_{h_n} + p\Delta t \, v_h \tag{16}$$

where p are all the future epochs up to the 15 second lookahead time.

5. *Hazard State Estimate and Estimate Error Variance*

The trajectory state estimator produces a trajectory state estimate, $\hat{\mathbf{x}}_n$, and a Kalman filter estimate error covariance matrix, $\hat{\mathbf{P}}_n$. The hazard state estimate vector, $\hat{\boldsymbol{\psi}}_n$, at epoch n is:

$$\hat{\boldsymbol{\psi}}_n = \begin{bmatrix} \hat{\tau}_{mod,n} & \hat{r}_{CPA,n} & \hat{h}_{p,n} \end{bmatrix}^T \tag{17}$$

A first order Taylor series expansion is used to obtain the linearized approximation of the hazard state estimates in relation to the trajectory state estimates ($\hat{\mathbf{x}}_n$):

$$\hat{\boldsymbol{\psi}}_n \approx \mathbf{A}_n \hat{\mathbf{x}}_n \tag{18}$$

where $\mathbf{A}_n$ represents the Taylor Series partial derivative vectors ($\mathbf{a}_{\tau_n}^T$, $\mathbf{a}_{r_n}^T$, $\mathbf{a}_{h_n}^T$) stacked into one matrix:

$$\mathbf{A}_n = \begin{bmatrix} \mathbf{a}_{\tau_n}^T \\ \mathbf{a}_{r_n}^T \\ \mathbf{a}_{h_n}^T \end{bmatrix} \tag{19}$$

As an example of the partial derivative vectors, $\mathbf{a}_{\tau_n}^T$ is the vector of partial derivatives of τ_{mod} with respect to the trajectory states (for constant velocity):

$$\mathbf{a}_{\tau_n}^T = \begin{bmatrix} \frac{\partial \tau_{mod,n}}{\partial d_{x_n}}\Big|_{\bar{\mathbf{x}}} & \frac{\partial \tau_{mod,n}}{\partial d_{y_n}}\Big|_{\bar{\mathbf{x}}} & \frac{\partial \tau_{mod,n}}{\partial d_{h_n}}\Big|_{\bar{\mathbf{x}}} & \frac{\partial \tau_{mod,n}}{\partial v_x}\Big|_{\bar{\mathbf{x}}} & \frac{\partial \tau_{mod,n}}{\partial v_y}\Big|_{\bar{\mathbf{x}}} & \frac{\partial \tau_{mod,n}}{\partial v_h}\Big|_{\bar{\mathbf{x}}} \end{bmatrix} \tag{20}$$

where $\bar{\mathbf{x}}$ is an a-priori estimate of the trajectory states. The partial derivative vectors $\mathbf{a}_{r_n}^T$ and $\mathbf{a}_{h_n}^T$ are found in the same manner.

The full covariance matrix, $\mathbf{P}_{\psi_n}$, of the hazard state estimate vector, $\hat{\boldsymbol{\psi}}_n$, is determined by the following:

$$\mathbf{P}_{\psi_n} = \mathbf{A}_n \hat{\mathbf{P}}_n \mathbf{A}_n^T \tag{21}$$

$\mathbf{P}_{\psi_n}$ is fully populated so the hazard state estimates ($\hat{\tau}_{mod}$, $\hat{r}_{CPA}$, and $\hat{h}_p$) are correlated. The hazard state estimate variances (σ_τ^2, σ_r^2, and σ_h^2) are the diagonal elements of $\mathbf{P}_{\psi_n}$.

B. Hazard States with Constant Accelerations

Removing the constant velocity assumption adds another level of complexity to the SAA problem. Because the acceleration is linear, the trajectory geometry does not change relative to the constant velocity case, and the geometric horizontal CPA in equation (14) is still valid. However, the modified tau in equation (8) and the predicted vertical separation in equation (16), must be refined. Therefore we introduce an adjusted true tau and an adjusted predicted vertical separation to augment the existing constant velocity versions of τ_{mod} and h_p.

1. True Tau Adjusted for Accelerations

The expressions for the Cartesian breakdown of horizontal CPA position, x_{CPA} and y_{CPA}, are as follows:

$$x_{CPA} = d_x + v_x \tau_{true} + \frac{1}{2} a_x \tau_{true}^2 \tag{22}$$

$$y_{CPA} = d_y + v_y \tau_{true} + \frac{1}{2} a_y \tau_{true}^2 \tag{23}$$

Because the direction of the velocity does not change and remains perpendicular to $\mathbf{r}_{CPA}$, the vector from the own aircraft to the CPA, the dot product of equation (10) holds:

$$x_{CPA}v_x + y_{CPA}v_y = 0 \tag{24}$$

This results in the following quadratic:

$$v_x(d_x + v_x\tau_{true} + \frac{1}{2}a_x\tau_{true}^2) + v_y(d_y + v_y\tau_{true} + \frac{1}{2}a_y\tau_{true}^2) = 0 \tag{25}$$

Written another way:

$$(\frac{v_xa_x + v_ya_y}{2})\tau_{true}^2 + (v_x^2 + v_y^2)\tau_{true} + (d_xv_x + d_yv_y) = 0 \tag{26}$$

Solving for τ_{true}, the new true tau becomes:

$$\tau_{true} = \frac{-(v_x^2 + v_y^2) + \sqrt{(v_x^2 + v_y^2)^2 - 2(v_xa_x + v_ya_y)(d_xv_x + d_yv_y)}}{v_xa_x + v_ya_y} \tag{27}$$

2. Predicted Vertical Separation Adjusted for Accelerations

The predicted vertical separation equation (16) now needs to be adjusted for constant accelerations resulting in the following equation:

$$h_p = d_{h_n} + p\Delta tv_h + \frac{(p\Delta t)^2}{2}a_h \tag{28}$$

where Δt is the sample rate and p represents all the future epochs up to the 15 second lookahead time that defines a late alert [10].

III. Relating Integrity and Continuity to Sensor Requirements

The previous work [13] has a detailed explanation of the the methodology for establishing probability multipliers corresponding to predefined integrity and continuity risk requirements. These coefficients are then multiplied by hazard state estimate standard deviations to provide WCT adjustments which, in this work, account for both sensor noise and intruder acceleration uncertainty. The hazard state estimate standard deviations are σ_τ for time to horizontal CPA, σ_r for horizontal CPA, and σ_h for predicted vertical separation. The multiples are k_τ, k_r, and k_h for integrity risk and ℓ_τ, ℓ_r, and ℓ_h for continuity risk.

A. Integrity Risk

As outlined in the previous work [13], the integrity risk, or the probability of hazardously misleading information (HMI), P_{HMI}, is based on the following bounds [13]:

$$P_{HMI} \leq Q(k_\tau) + Q(k_r) + Q(k_h) + Q(k_h + 1) \tag{29}$$

$$Q(k_\tau) + Q(k_r) + Q(k_h) + Q(k_h + 1) \leq I_{SS} \tag{30}$$

where integrity risk is bounded by a sum of Q-functions which we want to ensure is bounded by the certification authority-specified integrity requirement, I_{SS}. A Q-function is the tail probability of the standard normal distribution. This allows us to select integrity coefficients, k's, based on the integrity risk requirement, I_{SS}. These k's are used to create an integrity-adjusted protection level around the Hazard Zone (or WCT), by adding $k\sigma$ to each hazard state threshold.

HMI is an unacceptably large error without a timely warning that the system cannot be trusted [42]. For the SAA problem, HMI occurs when the SAA system is providing misleading information by not sensing a hazard (due to large sensor errors) while a hazard is actually present and a self-separation maneuver is required. The probability of HMI is reflected in equation (31):

$$P_{HMI} = P(\text{Sense No Hazard}|\text{Hazard Exists}) \tag{31}$$

In equation (31), the condition reflects an imminent (at or within τ^*_{mod} seconds) WCT violation (or loss of DWC) at the warning alert limit. **Hazard Exists** describes a condition where three events are predicted to ***occur simultaneously***:

- Actual time to CPA, τ_{mod}, is less than or equal to τ^*_{mod},
- ***and*** actual horizontal CPA, r_{CPA}, is at or within HMD^*,
- ***and*** actual predicted vertical separation, h_p, is at or within $\pm h^*$.

In this case, the own aircraft should initiate a self-separation maneuver. **Sense No Hazard** describes a case where ***any*** of the following four events is occurring:

- Estimated time to CPA, $\hat{\tau}_{mod}$, is greater than the adjusted threshold $\tau^*_{mod} + k_\tau\sigma_\tau$,
- ***or*** estimated horizontal CPA, $\hat{r}_{CPA}$, is beyond the adjusted threshold $HMD^* + k_r\sigma_r$,
- ***or*** estimated predicted vertical separation, $\hat{h}_p$, is above the adjusted threshold $h^* + k_h\sigma_h$,
- ***or*** estimated predicted vertical separation, $\hat{h}_p$, is below the adjusted threshold $-h^* - k_h\sigma_h$.

Any one of these misleading estimates can cause HMI that leads the own aircraft to not maneuver when a self-separation maneuver is warranted.

B. Continuity Risk

Likewise, as outlined in the previous work [13], the continuity risk, or the probability of early alert (EA), P_{EA}, is based on the following bounds:

$$P_{EA} \leq \frac{\Phi(-\ell_\tau) + \Phi(-\ell_r) + \Phi(-\ell_h)}{3} \tag{32}$$

$$\frac{\Phi(-\ell_\tau) + \Phi(-\ell_r) + \Phi(-\ell_h)}{3} \leq C_{SS} \tag{33}$$

where $\Phi(x)$ represents the standard normal cumulative distribution function. This allows us to select continuity coefficients, ℓ's, based on the continuity risk requirement, C_{SS}. These ℓ's are used to create a continuity buffer within the Non-Hazard Zone (where the SAA system must not alert), by subtracting $\ell\sigma$ from each Non-Hazard Zone threshold.

The probability of EA is the probability of an early alert in the Non-Hazard Zone. The Non-Hazard Zone warning alert thresholds are defined in Table 1, with a modified tau (τ^*_{NHZ}) of 90 seconds, a horizontal miss distance (HMD^*_{NHZ}) of 1 NM, and a vertical separation (h^* or V_{mod}) of 450 feet [10]. The DAA MOPS defines the vertical portion of the Non-Hazard Zone as $|d_h| < V$, where the Vertical Proximity (V) is defined as [10]:

$$V = \max\left(V_{mod}, V_{mod} - \dot{h}\tau^*_{mod}\right) \tag{34}$$

For vertically converging trajectories (where the vertical closure, $\dot{h}$, is negative), the vertical Non-Hazard Zone threshold is $h^*_{NHZ} = V_{mod} - \dot{h}\tau^*_{mod}$. However, for level intruder trajectories (where $\dot{h} = 0$), the vertical Hazard Zone and Non-Hazard Zone thresholds are equal ($h^* = h^*_{NHZ} = V_{mod}$). Here, perfect sensors are required to differentiate between the two zones. We are concerned with non-cooperative intruders, where the DAA MOPS provides radar-only guidance that an intruder estimated to be within 3000 feet vertically will be treated as co-altitude [10]. To provide a margin between the vertical Hazard and Non-Hazard Zones for level intruders, we use a vertical separation threshold of 450 feet ($h^* = 450$ft) and a Non-Hazard Zone threshold of 3000 feet ($h^*_{NHZ} = 3000$ft).

In equation (35), the condition reflects a sensed WCT violation in the Non-Alert Zone.

$$P_{EA} = P(\text{Sense Hazard}|\text{No Hazard Exists}) \tag{35}$$

Sense Hazard describes a condition where three events ***occur simultaneously***:

- Estimated time to CPA, $\hat{\tau}_{mod}$, is less than or equal to $\tau^*_{mod} + k_\tau\sigma_\tau$,
- ***and*** estimated horizontal CPA, $\hat{r}_{CPA}$, is at or within $HMD^* + k_r\sigma_r$,
- ***and*** estimated predicted vertical separation, $\hat{h}_p$, is at or within $\pm(h^* + k_h\sigma_h)$.

No Hazard Exists describes a case where ***any*** of the following four events is occurring:

- Actual time to CPA, τ_{mod}, is greater than the Non-Hazard threshold τ^*_{NHZ},

- ***or*** actual horizontal CPA, $\hat{r}_{CPA}$, is beyond the Non-Hazard threshold HMD^*_{NHZ},
- ***or*** actual predicted vertical separation, $\hat{h}_p$, is above the Non-Hazard threshold h^*_{NHZ},
- ***or*** actual predicted vertical separation, $\hat{h}_p$, is below the negative Non-Hazard threshold $-h^*_{NHZ}$.

Any one of these early alerts can cause the own aircraft to maneuver when a self-separation maneuver is not warranted.

C. Operational Limits

With predefined integrity risk and continuity risk requirements, the SAA system's ability to alert will depend on how large each hazard state standard deviation (σ_τ, σ_r, σ_h) is at each sampled time. As the SAA system gets more intruder measurements, each hazard state standard deviation will get smaller over time.

The integrity adjustment ($k\sigma$) and the continuity buffer ($\ell\sigma$) are depicted for an encounter in Figure 3. These multiples of standard deviations must be small enough to fit into the space between the Hazard Zone and the Non-Hazard Zone. In the first frame of Figure 3, the intruder is initially detected at the initial position, $\mathbf{x}_0$. Here, σ is large and the integrity adjustment ($k\sigma$) and the continuity buffer ($\ell\sigma$) overlap with each other, resulting in no opportunity for the SAA system to alert and simultaneously meet integrity and continuity requirements. In the second frame of Figure 3, several measurements have been taken and σ is just small enough for the integrity adjustment and the continuity buffer to fit simultaneously within the Alert Zone. At this point, the system can start alerting for a predicted loss of DWC. Finally, in the last frame of Figure 3, σ is small, resulting in a larger margin to meet integrity and continuity requirements.

The SAA hazard detection test can be carried out with required integrity and continuity when all hazard state σ's decrease below their respective operational limits ($\tilde{\sigma}$'s), which is when the SAA system is available for alerting, as in frame two of Figure 3. The hazard state estimate standard deviation operational limits, $\tilde{\sigma}$'s, are defined by the following:

$$\tilde{\sigma}_\tau = \frac{\tau^*_{NHZ} - \tau^*_{mod}}{k_\tau + \ell_\tau} \tag{36}$$

$$\tilde{\sigma}_r = \frac{HMD^*_{NHZ} - HMD^*}{k_r + \ell_r} \tag{37}$$

$$\tilde{\sigma}_h = \frac{h^*_{NHZ} - h^*}{k_h + \ell_h} \tag{38}$$

where the Hazard Zone thresholds (τ^*_{mod}, HMD^*, and h^*), the Non-Hazard Zone thresholds (τ^*_{NHZ}, HMD^*_{NHZ}, and h^*_{NHZ}), the integrity coefficients (k_τ, k_r, and k_h), and the continuity coefficients (ℓ_τ, ℓ_r, and ℓ_h) have all been previously defined.

Not all SAA sensors or sensor-suites are capable of ensuring that the SAA system is available for alerting in time to perform a hazard detection test (with required integrity and continuity) before a hazard actually occurs. To identify sensors that can meet this requirement, an operational limit on true τ, $\tilde{\tau}$, is defined. This operational limit on true τ is

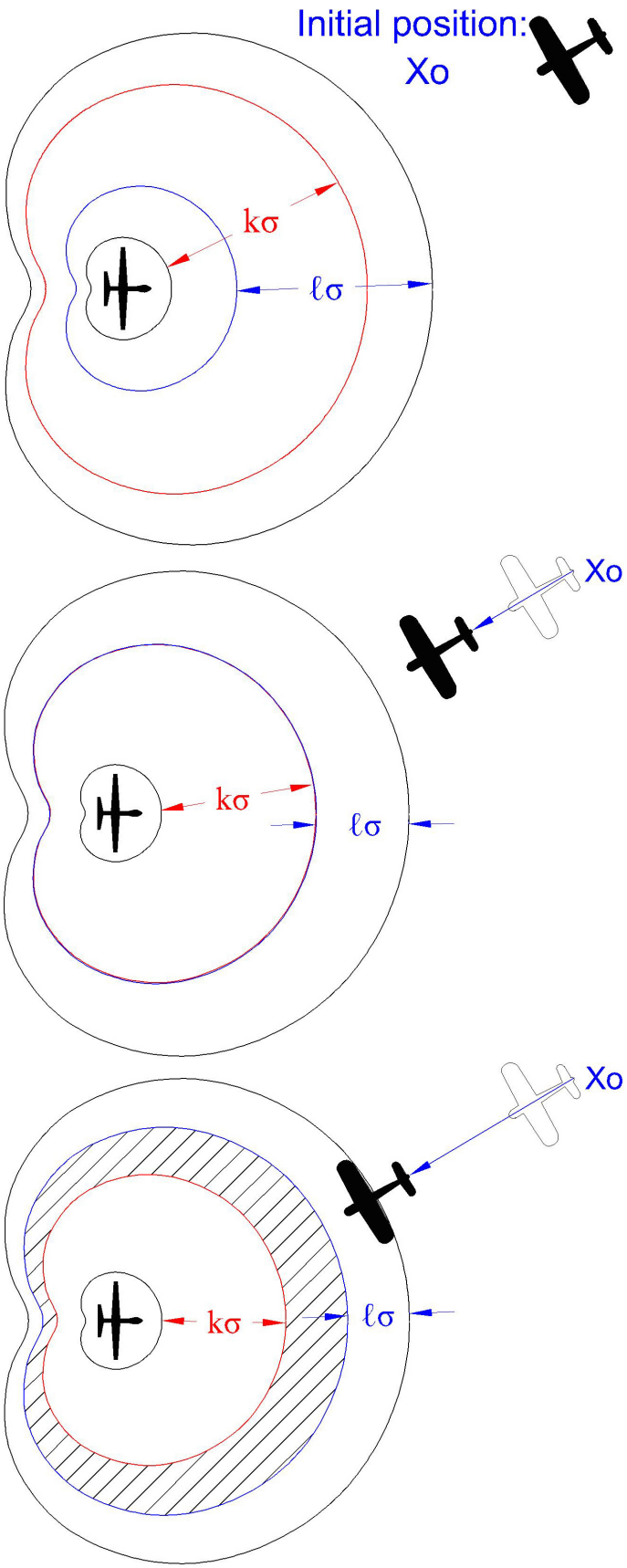

Figure 3. Encounter Progressing in Time: Decreasing σ Leads to Tighter Integrity Adjustments and Continuity Buffers

based on the DAA MOPS requirement to provide a warning alert at least 15 seconds prior to an intruder entering the Hazard Zone [10]:

$$\tilde{\tau} = \tau^*_{mod} + 15 \text{ seconds} \tag{39}$$

This results in a $\tilde{\tau}$ of 50 actual seconds (as measured using the true time to CPA), as opposed to "τ_{mod} seconds" (approximated using the τ_{mod} equation). This temporal operational limit will be applied to all hazard states.

Figure 4 depicts how the operational limit relates to sensor requirements. Each plot is a hazard state estimate standard deviation versus true tau, chosen as a convenient measure of time for the encounter. Each hazard state has its own plot and within each plot there are three curves representing three different sensors. For a sensor to meet requirements, each of its σ curves, for each of its hazard states, must be less than its $\tilde{\sigma}$ at a true τ greater than $\tilde{\tau}$. If any of the sensor's σ curves cross its respective $\tilde{\sigma}$ at a true τ less than $\tilde{\tau}$ (and penetrates the gray shaded area), that sensor will not meet continuity and integrity risk requirements. In the figure, only the bottom sensor, Sensor 3, meets the continuity risk and integrity risk requirements.

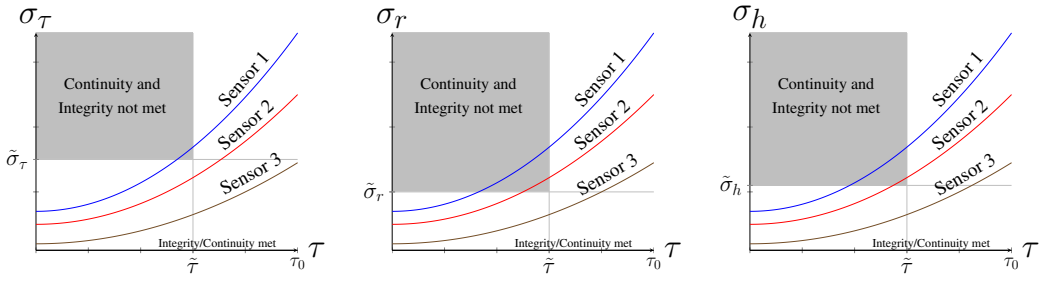

Figure 4. Applying Operational Limits to Sensor Requirements

In order to apply this methodology, a sensor must have characteristics (measurement uncertainty, sensor range, and sample interval) to reduce each hazard state estimate error standard deviation below its operational limit $\tilde{\sigma}$ prior to its true τ operational limit, $\tilde{\tau}$, as depicted for Sensor 3 in Figure 4. If a given sensor is not good enough, sensor error must be reduced, sensor range must be extended, and/or the intervals between independent samples must be reduced. In order to maintain continuity, a minimal number of self-separation tests must be accomplished. For a constant velocity model, once all three hazard state estimate error standard deviations are reduced below their operational limits, $\tilde{\sigma}$'s, there only needs to be one test for a warning alert.

D. Recap of Equations

The following is a final recap of derived and pertinent equations from this section.

The bounds on integrity risk are:

$$P_{HMI} \leq Q(k_\tau) + Q(k_r) + Q(k_h) + Q(k_h + 1) \tag{40}$$

$$Q(k_\tau) + Q(k_r) + Q(k_h) + Q(k_h + 1) \leq I_{SS} \tag{41}$$

The bounds on continuity risk are:

$$P_{EA} \leq \frac{\Phi(-\ell_\tau) + \Phi(-\ell_r) + \Phi(-\ell_h)}{3} \tag{42}$$

$$\frac{\Phi(-\ell_\tau) + \Phi(-\ell_r) + \Phi(-\ell_h)}{3} \leq C_{SS} \tag{43}$$

The operational limits on the hazard state estimate error standard deviations are:

$$\tilde{\sigma}_\tau = \frac{\tau^*_{NHZ} - \tau^*_{mod}}{k_\tau + \ell_\tau} \tag{44}$$

$$\tilde{\sigma}_r = \frac{HMD^*_{NHZ} - HMD^*}{k_r + \ell_r} \tag{45}$$

$$\tilde{\sigma}_h = \frac{h^*_{NHZ} - h^*}{k_h + \ell_h} \tag{46}$$

Finally, the temporal operational limit is:

$$\tilde{\tau} = \tau^*_{mod} + 15 \text{ seconds} \tag{47}$$

IV. Sensitivity Analysis

There are two parts to this sensitivity analysis, a 3D analysis, which is an extension of the previous 2D analysis of the previous work [13], and an analysis of the intruder linear accelerations.

A. Nominal Composite Sensor

The same nominal sensor is used for all analyses in this section. In the draft DAA MOPS, the input intruder measurements from an SAA radar includes relative slant range (ρ), relative range rate ($\dot{\rho}$), relative bearing (θ), and elevation angle (ϕ) [10]. The nominal sensor will be assumed to measure ρ, $\dot{\rho}$, θ, and ϕ. Chen, et al., described nominal characteristics for SAA sensors, reproduced in Table 2 [56]. This table includes cooperative and non-cooperative sensors. The cooperative sensors are the Traffic Collision Avoidance System (TCAS) and Automatic Dependent Surveillance-Broadcast (ADS-B). The non-cooperative sensors in this table are airborne radar and electro-optical (EO). This research is concerned with non-cooperative sensors. The radar accuracy is defined in terms of range, range rate, azimuth angle and elevation angle. The electro-optical accuracy is defined in terms of azimuth and elevation angles. Chen does not define a range accuracy for electro-optical sensors explaining that "EO (monoscopic) does not inherently generate range information and the detection range is typically poor" [56].

For non-cooperative SAA intruder sensor measurements, SC-228 developed a draft MOPS for Air-to-Air Radar

Table 2. SAA Sensor Characteristics [56]

	TCAS	ADS-B	Radar	Electro-optical
Accuracy	ρ: 175 - 300 ft θ: 9 - 15 deg h: 50 - 100 ft	x, y: 25 - 250 ft h: 50 - 100 ft	θ: 0.5 - 2° ϕ: 0.5 - 2° ρ: 10 - 200 ft $\dot{\rho}$: 1 - 10 $\frac{ft}{s}$	θ: 0.1 - 0.5° ϕ: 0.1 - 0.5°
Update rate	1 Hz	1 Hz	0.2 - 5 Hz	20 Hz
Detection range	$\geq$ 14 NM	$\geq$ 20 NM	5 - 10 NM	2 - 5 NM

DAA Systems, which specifies the non-cooperative SAA radar sensor will have the following maximum standard deviations: σ_ρ = 50 feet, σ_θ = 1°, σ_ϕ = 1°, and $\sigma_{\dot{\rho}}$ = 10 ft/s [57]. The sensor detection range, ρ_0, is 8 nautical miles (NM), derived from MIT Lincoln Laboratory research, the DAA MOPS and the Air to Air Radar DAA MOPS [58, 31, 10, 57]. All these radar parameters are within Chen's radar characteristic range from Table 2. The nominal sample rate, Δt, is 1 Hz, taken directly from the DAA MOPS [10, 57]. In aviation, distance is typically measured in nautical miles, airspeed is typically measured in knots (nautical miles per hour), and altitude is measured in feet. Given the aviation application of this research, these units will be used instead of the International System of Units (SI).

The assumed well clear threshold is based on the warning alert Hazard Zone and Non-Hazard Zone thresholds from the DAA MOPS [10]. The desired integrity requirement, $I_{SS} = 10^{-6}$, and the continuity requirement, $C_{SS} = 10^{-3}$, are based on the FAA's definition of major and minor failure conditions [59]. The major condition for integrity is based on the DAA White Paper's working assumption that the failure classification of DAA equipment will be "severe major" [12]. The minor condition for continuity, which includes nuisance alerts, comes from the FAA's AC 25.1309-1A, which describes a nuisance as a consequence of a probable, minor failure condition [59]. All parameters for the nominal sensor is listed in Table 3.

Table 3. Nominal Sensor for Analyses

Characteristic	Value
Range Uncertainty, σ_ρ	50 feet
Azimuth Uncertainty, σ_θ	1.0°
Elevation Uncertainty, σ_ϕ	1.0°
Range Rate Uncertainty, $\sigma_{\dot{\rho}}$	10 ft/s
Detection Range, ρ_0	8 NM
Sample Rate, Δt	1 Hz
Integrity Requirement, I_{SS}	10^{-6}
Continuity Requirement, C_{SS}	10^{-3}

B. Three Dimensional Trajectories

The 3D analysis focuses on seven trajectories, which were originally analyzed in previous work [14] for earlier definitions of the hazard states and WCT. The intent of this analysis is to examine these seven trajectories as border cases as an example of how to successfully apply the methodology. Future work will include deeper analysis of like-

lihood of encounter types, based on encounter models, to the integrity risk and continuity risk analyses and to provide comparisons to prior risk ratio methodologies, such as the 2013 MIT Lincoln Laboratory analysis in [60].

These seven trajectories are:

- Head-on, direct collision course descending.
- Head-on, level at h^*.
- Tangent to the HMD^* circle, level at h^*.
- Head-on, descending, intercepting the top WCT border at the back.
- Tangent to the HMD^* circle, descending, intercepting the top WCT border.
- Head-on, descending, intercepting the bottom WCT border at the front.
- Tangent to the HMD^* circle, descending, intercepting the bottom WCT border.

A side view of the head-on trajectories are depicted in the left side of Figure 5 and a top down view of the head-on and tangent trajectories are depicted on the right side of Figure 5.

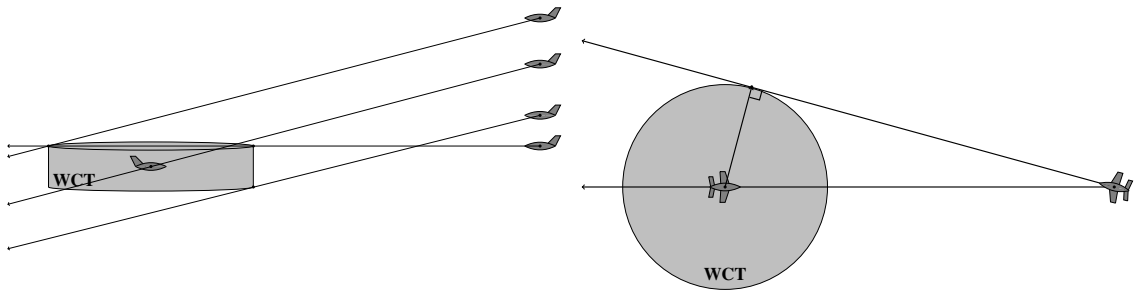

Figure 5. Three Dimensional Trajectories

These trajectories were selected based on the worst-case trajectories in 2D (determined from the previous work [13]) being head-on and tangent and the vertical profiles were based on level and descending border cases around the WCT cylinder. Based on the DAA MOPS, the maximum relative descent rate is 5000 feet per minute (fpm) and the maximum relative closure velocity is limited to 370 knots for non-cooperative intruders [10]. Also, for simplicity, the integrity and continuity risk coefficients are set to be equal: $k_\tau = k_r = k_z = 4.98$ and $\ell_\tau = \ell_r = \ell_z = 3.09$. From these integrity and continuity multipliers, the corresponding operational limits are $\tilde{\sigma}_\tau = 6.82$ seconds, $\tilde{\sigma}_r = 256.0$ feet, and $\tilde{\sigma}_h = 316.0$ feet. For σ_a, we choose 0.33 knot/s, based on a maximum 3-σ intruder acceleration of 1 knot/s taken from the intruder aircraft behavior distribution of the MIT Lincoln Laboratory Uncorrelated Encounter Model for the NAS, which is, in turn, based on extensive radar data collection from over 120 sensors nation-wide of general aviation VFR aircraft [10, 53, 54].

C. Constant Velocity 3D Results

The results from the nominal case are in Figure 6. In this section, τ without a subscript (as is the τ on the x-axis of the plots) is the true tau from equation (27). In other words, in these plots, the curve for the most restrictive trajectory is illustrated. Integrity and continuity are met if each σ vs τ curve stays out of the gray shaded, upper left quadrant of the plots. The horizontal line is the $\tilde{\sigma}$ operational limit and the vertical line is the $\tilde{\tau}$ operational limit. Note that time goes from right (representing the initial tau at the detection range, τ_0) to left (representing the final tau at the CPA, $\tau_{CPA} = 0$).

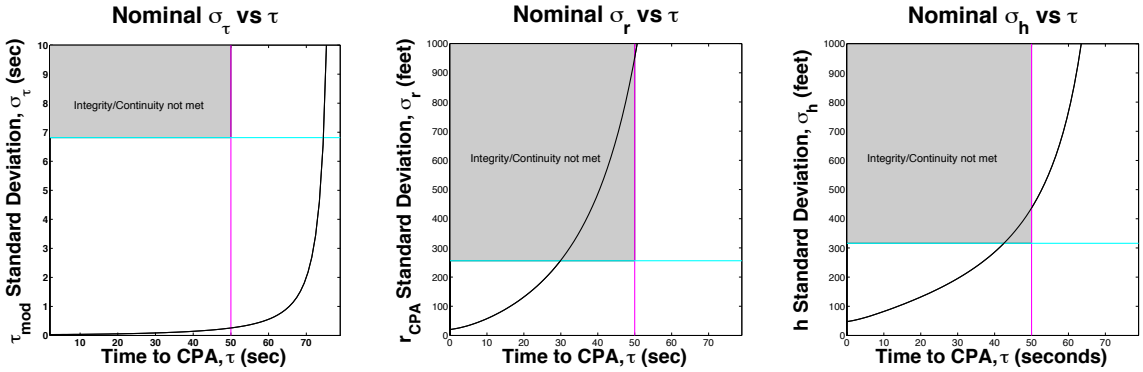

Figure 6. 3D Results of a Nominal Sensor

For this nominal sensor, all trajectories meet the σ_τ requirements for integrity and continuity, but none of the trajectories meet requirements for σ_r and σ_h. In the σ_τ case, performance is similar for all trajectories and the curves fall below the $\tilde{\sigma}_\tau$ operational limit within the first few time-epochs. In the σ_r and σ_h cases, performance is also similar for all trajectories, but the curves fall below the $\tilde{\sigma}$ horizontal lines to the left of the $\tilde{\tau}$ operational limit, suggesting a sensor with better performance is required.

1. *Sensor Adjustments*

The standard deviations σ_r and σ_h are sensitive to azimuth and elevation measurement errors. Improving the nominal radar sensor with adjustments in azimuth and elevation can result in an SAA system that can meet integrity and continuity requirements. To demonstrate this, azimuth and elevation uncertainty are improved to σ_θ = 0.25°, σ_ϕ = 0.7°, reflecting a radar with improved performance at the end of the range Chen described in Table 2 [56].

The results from the adjusted sensor are in Figure 7. Now, the sensor meets integrity and continuity requirements for all three hazard states (barely meeting the requirements for the horizontal and vertical hazard states).

D. 3D Results: Accelerations and Uncertainty in Intruder Pilot Thrust

Going back to using the nominal sensor, now the predicted standard deviation on intruder acceleration is applied. This standard deviation, σ_a, is selected to be 0.33 knots/sec, based on a maximum 3-σ intruder acceleration of 1 knot/s

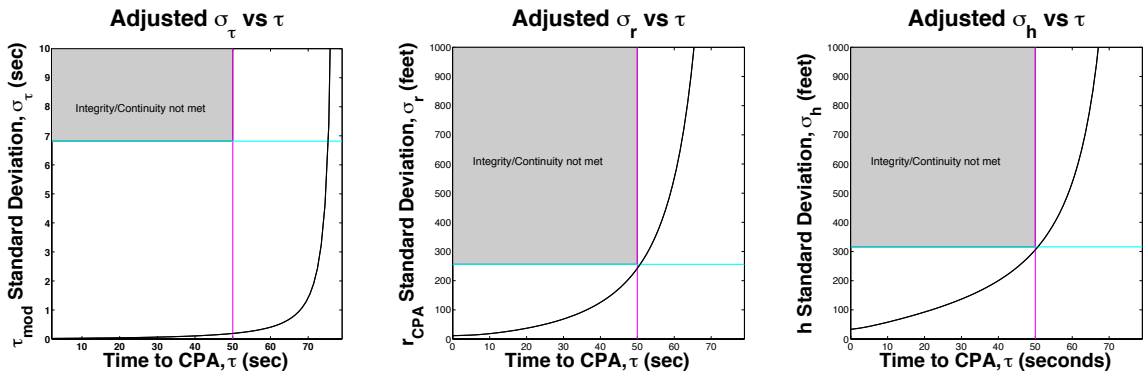

Figure 7. 3D Results of an Adjusted Sensor

taken from the intruder aircraft behavior distribution of the MIT Lincoln Lab Uncorrelated Encounter Model for the NAS [10, 53, 54]. Each trajectory with this σ_a = 0.33 knots/sec will be compared to the case with assumed perfect knowledge of the intruder pilot acceleration, where $\sigma_a = 0$.

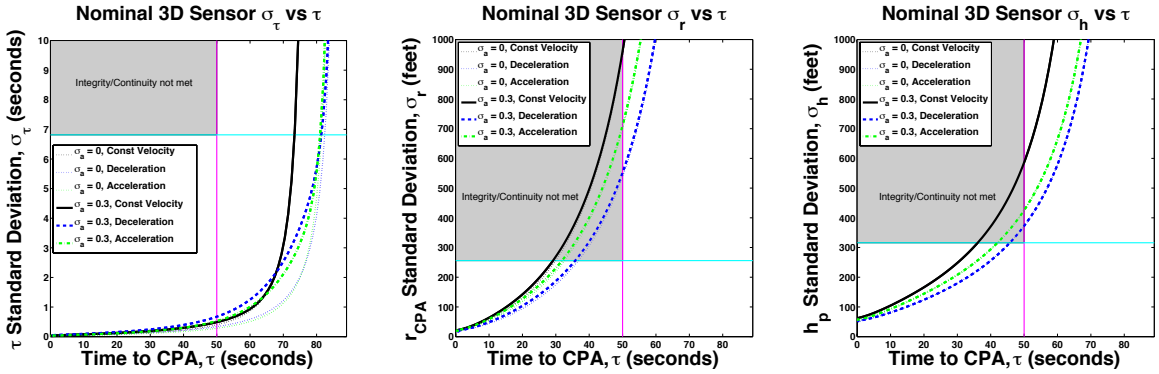

Figure 8. Linear Acceleration Results of a Nominal Sensor

The results of the nominal sensor is in Figure 8. As in the constant velocity case of the previous subsection, the nominal sensor meets τ requirements for all trajectories and accelerations. Also, in a similar manner to the constant velocity case, the nominal sensor does not meet horizontal and vertical separation requirements. The only difference of note is that the accelerated trajectories result in longer times (and more measurements) within the sensor range than the constant velocity case, because the latter is always at maximum velocity. As for the impact of accounting for an unknown intruder thrust action, it is minimal with respect to σ_r, mostly because r_{CPA} is a function of position and velocity only, and is minimal with respect to σ_h, because the linear acceleration results in a maximum vertical acceleration of only $a_h = 0.23\frac{ft}{s^2}$.

There is a notable difference between τ_{mod} and the true tau that accounts for accelerations, depicted in Figure 9. Since the expression for τ_{true} includes the constant acceleration states, it is more accurate than τ_{mod} which is an approximation that only includes position and velocity states. The TCAS II MOPS described the D_{mod} term in τ_{mod}

as a "safety factor incorporated in range measurements to account for possible accelerations by the intruder" [55]. The τ_{true} curves separated at earlier epochs into a more restrictive position (closer to the upper left quadrant whose boundary signifies the integrity and continuity risk requirement) than the τ_{mod} curves, despite both cases having an ample margin of safety between integrity and continuity requirements.

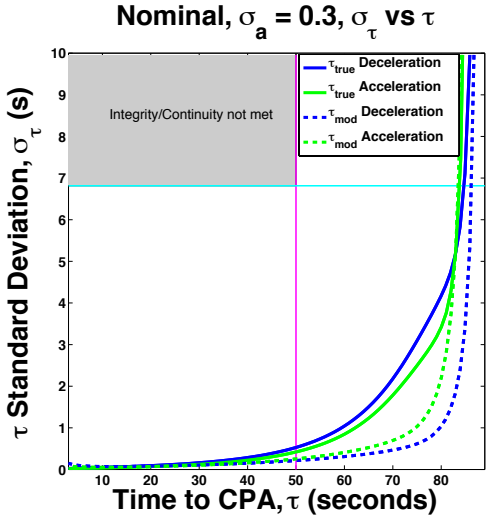

Figure 9. Linear Acceleration Nominal Sensor Tau Comparison

As in the constant velocity case, the sensor can be adjusted to meet integrity and continuity requirements. An example of this is in Figure 10. Here, the azimuth and elevation uncertainty are improved to $\sigma_\theta = 0.25°$, $\sigma_\phi = 0.5°$. Now, as in the constant velocity case, the sensor does meet integrity and continuity requirements. This is an example of exploring the sensor requirement trade space.

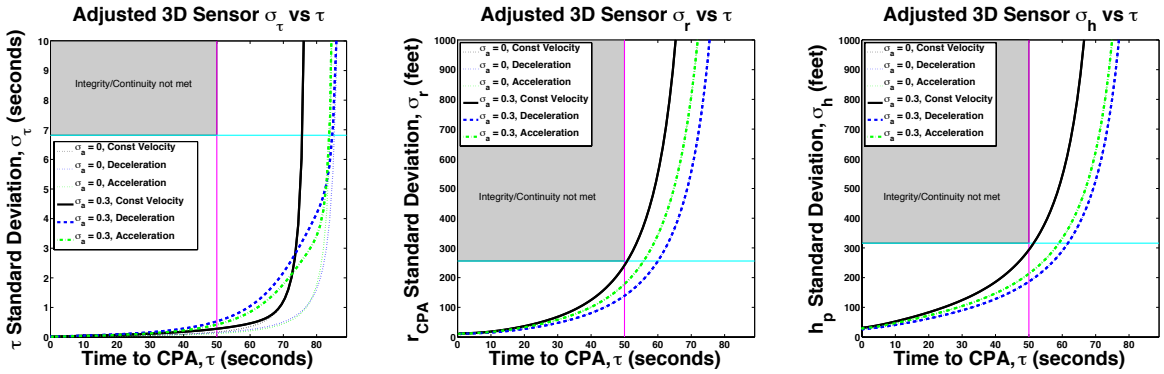

Figure 10. Linear Acceleration Results of an Adjusted Sensor

V. Conclusions

In this paper, we determined integrity and continuity risk for straight line intruder accelerations. A sensitivity analysis was presented to explore the sensor requirement trade space and analyze 3D accelerating trajectories. We were able to adjust sensor characteristics in the analysis to explore the trade space while meeting integrity and continuity requirements. The uncertainties in straight line intruder dynamics impacted τ only (while still easily meeting τ integrity and continuity requirements) and negligibly impacted the other hazard states. Our methodology can be used by a certification authority to certify potential SAA sensors. Opportunities for future work include adding turning trajectories, accounting for wind gusts, and considering multiple intruders.

Appendix

Estimation Model

The sense and avoid problem is presented as a three dimensional, two-body problem. The two bodies are the own aircraft and the intruder aircraft. The coordinate frame is an own-aircraft-centered body frame. Figure 11 is a graphical depiction of the own aircraft and the intruder aircraft encounter looking down from the top (on the left) and looking from the side (on the right). In the horizontal plane, the x and y axes are oriented such that the x-axis is directly out of the nose of the own aircraft. The azimuth, θ, is the angle counterclockwise from the x-axis to the horizontal range vector, $\mathbf{r}$ (from the origin to the intruder position on the xy-plane). In the vertical plane, ϕ is the elevation angle from the horizontal range vector up to the slant range vector, $\boldsymbol{\rho}$:

$$\cos\phi = \frac{r}{\rho} \tag{48}$$

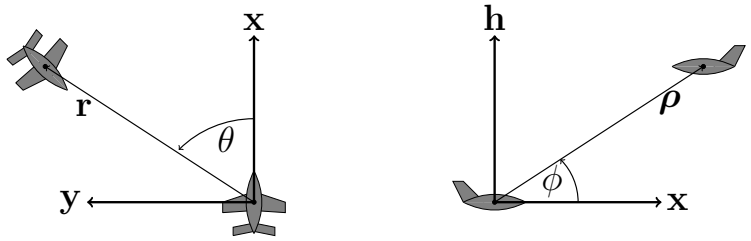

Figure 11. Horizontal and Vertical Position of the Intruder Aircraft

The intruder *trajectory states*, $\mathbf{x}_n$, are the relative Cartesian intruder position and constant velocity:

$$\mathbf{x}_n = \begin{bmatrix} d_{x_n} & d_{y_n} & d_{h_n} & v_x & v_y & v_h \end{bmatrix}^T \tag{49}$$

where n is the current epoch. The constant velocity assumption here is based on the draft DAA MOPS, where it is

assumed that intruder track prediction will be extrapolated using constant velocity [10].

SAA sensors can measure the intruder's relative position (with error) in spherical, Cartesian, or cylindrical coordinates. In the draft Detect and Avoid Minimum Operational Performance Standards, the input intruder measurements from a sense and avoid radar includes relative slant range (ρ), relative range rate ($\dot{\rho}$), relative bearing (θ), and elevation angle (ϕ) [10]. As a result, this paper assumes intruder measurements ($\mathbf{z}_n$) of range, range rate, azimuth angle and elevation angle as expressed in equation (50):

$$\mathbf{z}_n = \begin{bmatrix} \rho_n & \theta_n & \phi_n & \dot{\rho}_n \end{bmatrix}^T \tag{50}$$

Measurement Model

The own aircraft makes a scan at time n measuring the the intruder position:

$$\mathbf{z}_n = \mathbf{h}(\mathbf{x}_n) + \mathbf{v}_n \qquad \mathbf{v}_n \sim N(\mathbf{0}, \mathbf{V}_n) \tag{51}$$

$\mathbf{z}_n$ is the measurement at time n, expressed in equation (50), which is a nonlinear function ($\mathbf{h}(\mathbf{x}_n)$) of the trajectory states ($\mathbf{x}_n$) which are intruder Cartesian position and velocity. $\mathbf{v}_n$ is the measurement error, which is assumed to be over-bounded in the cumulative distribution function (CDF) sense by Gaussian distributions [61, 62]. The measurement error covariance matrix at each time is $\mathbf{V}_n$. In equation (51), $N(\mathbf{a}, \mathbf{B})$ represents a normal distribution with mean $\mathbf{a}$ and covariance $\mathbf{B}$. It is assumed that the sample interval, Δt, is selected large enough to ensure independence of sequential sensor measurement errors.

The measurement equation (51) can be linearized. Using a first order Taylor series:

$$\mathbf{h}(\mathbf{x}) \approx \mathbf{h}(\bar{\mathbf{x}}) + \mathbf{H}\delta\mathbf{x} \tag{52}$$

where $\mathbf{H}$ is the observation matrix:

$$\mathbf{H} = \frac{\partial \mathbf{h}}{\partial \mathbf{x}} \tag{53}$$

$\bar{\mathbf{x}}$ is an estimate of the trajectory states, and $\delta\mathbf{x}$ is the estimate error $\bar{\mathbf{x}} - \mathbf{x}$. Substituting into equation (51), $\mathbf{z}_n$ becomes:

$$\mathbf{z}_n \approx \mathbf{h}(\bar{\mathbf{x}}_n) + \mathbf{H}\delta\mathbf{x}_n + \mathbf{v}_n \tag{54}$$

Then expanding $\delta\mathbf{x}$ and putting all known quantities on the left hand side, $\mathbf{z}_n$ becomes:

$$\mathbf{z}_n - \mathbf{h}(\bar{\mathbf{x}}_n) + \mathbf{H}\bar{\mathbf{x}}_n \approx +\mathbf{H}\mathbf{x}_n + \mathbf{v}_n \tag{55}$$

Defining the left hand side of the equation to be $\mathbf{z}' \triangleq \mathbf{z} - \mathbf{h}(\bar{\mathbf{x}}) + \mathbf{H}\bar{\mathbf{x}}$, a linear measurement model is obtained:

$$\mathbf{z}'_n = \mathbf{H}\mathbf{x}_n + \mathbf{v}_n \tag{56}$$

Acknowledgments

We would like to express our appreciation to Phil Maloney, UAS Certification Obstacle Team Leader, of the FAA Hughes Technical Center, for supporting this research, which was awarded FAA Grant #14-G-018. However, the views expressed in this paper are the authors' alone and do not necessarily represent the opinions of any other organization or person.

References

[1] Federal Aviation Administration, "Integration of Civil Unmanned Aircraft Systems (UAS) in the National Airspace System (NAS) Roadmap," Nov 2013.

[2] US House of Representatives, "FAA Modernization and Reform Act of 2012," Feb 2012.

[3] Federal Aviation Administration TCAS Program Office, "Concept of Use for the Airborne Collision Avoidance System X_U," Sep 2015, Version 2, Revision 0.

[4] Federal Aviation Administration, "Sense and Avoid (SAA) for Unmanned Aircraft Systems (UAS), SAA Workshop Second Caucus Report," Jan 2013.

[5] Anderson, E. E., Watson, W., Johnson, K., Kimber, N. R., and Weiss, N. J., "A Legal Analysis of 14 C.F.R. Part 91 See and Avoid Rules to Identify Provisions Focused on Pilot Responsibilities to See and Avoid in the National Airspace System." Tech. rep., University of North Dakota-U.S. Department of Transportation, Federal Aviation Administration, Dec 2013.

[6] 14 CFR 91.113, "Right-of-way Rules: Except Water Operations," Jul 2004.

[7] Weibel, R. E., Edwards, M. W. M., and Fernandes, C. S., "Establishing a Risk-Based Separation Standard for Unmanned Aircraft Self Separation," *Ninth USA/Europe Air Traffic Management Research and Development Seminar*, Berlin, Germany, Jun 2011, pp. 1–7.

[8] Lee, S. M., Park, C., Johnson, M. A., and Mueller, E. R., "Investigating Effects of Well Clear Definitions on UAS Sense-And-Avoid Operations," *2013 Aviation Technology, Integration, and Operations Conference*, American Institute of Aeronautics and Astronautics (AIAA), Los Angeles, CA, Aug 2013, pp. 1–15.

[9] Cook, S. P., Brooks, D., Cole, R., Hackenberg, D., and Raska, V., "Defining Well Clear for Unmanned Aircraft Systems," *AIAA Infotech @ Aerospace*, American Institute of Aeronautics and Astronautics (AIAA), Kissimmee, FL, Jan 2015, pp. 1–20.

[10] RTCA SC-228, "Draft Detect and Avoid Minimum Operational Performance Standards for Verification and Validation, Version 3.3," Apr 2016.

[11] Federal Aviation Administration, "Advisory Circular 107-2 - Small Unmanned Aircraft Systems," Jun 2016.

[12] RTCA SC-228, "Detect and Avoid (DAA) White Paper," Mar 2014.

[13] Jamoom, M. B., Joerger, M., and Pervan, B., "Unmanned Aircraft System Sense-and-Avoid Integrity and Continuity Risk," *Journal of Guidance, Control, and Dynamics*, Vol. 39, No. 3, Mar 2016, pp. 498–509.

[14] Jamoom, M. B., Joerger, M., and Pervan, B., "Sense and Avoid for Unmanned Aircraft Systems: Ensuring Integrity and Continuity for Three Dimensional Intruder Trajectories," *Institute of Navigation GNSS+*, Tampa, FL, Sep 2015.

[15] RTCA SC-159, "Minimum Aviation System Performance Standards for the Local Area Augmentation System," Dec 2004.

[16] Kuchar, J. K. and Yang, L. C., "A Review of Conflict Detection and Resolution Modeling Methods," *IEEE Transactions on Intelligent Transportation Systems*, Vol. 1, No. 4, Dec 2000, pp. 179–189.

[17] Drumm, A., Andrews, J., Hall, T., Heinz, V., Kuchar, J., Thompson, S., and Welch, J., "Remotely Piloted Vehicles in Civil Airspace: Requirements and Analysis Methods for the Traffic Alert and Collision Avoidance System (TCAS) and See-And-Avoid Systems," *IEEE Digital Avionics Systems Conference*, Vol. 2, Salt Lake City, UT, Oct 2004, pp. 12.D.1–1–14.

[18] Dalamagkidis, K., Valavanis, K., and Piegl, L., "On Unmanned Aircraft Systems Issues, Challenges and Operational Restrictions Preventing Integration into the National Airspace System," *Progress in Aerospace Sciences*, Vol. 44, No. 7, Jul 2008, pp. 503–519.

[19] Prats, X., Delgado, L., Ramirez, J., Royo, P., and Pastor, E., "Requirements, Issues, and Challenges for Sense and Avoid in Unmanned Aircraft Systems," *AIAA Journal of Aircraft*, Vol. 49, No. 3, May 2012, pp. 677–687.

[20] Yu, X. and Zhang, Y., "Sense and Avoid Technologies with Applications to Unmanned Aircraft Systems: Review and Prospects," *Progress in Aerospace Sciences*, Vol. 74, Apr 2015, pp. 152–166.

[21] McLaughlin, M. P. and Zeitlin, A. D., "Safety Study of TCAS II for Logic Version 6.04," Tech. rep., MITRE Corporation-U.S. Department of Transportation, Federal Aviation Administration, Jul 1992.

[22] Espindle, L., Griffith, J., and Kuchar, J., "Safety Analysis of Upgrading to TCAS Version 7.1 Using the 2008 U.S. Correlated Encounter Model," Tech. rep., Lincoln Laboratory, Massachusetts Institute of Technology, May 2009.

[23] International Civil Aviation Organization, "ICAO 9689-AN/953 Manual on Airspace Planning Methodology for the Determination of Separation Minima," Dec 1998.

[24] Kim, J.-H., Lee, D. W., Cho, K.-R., Jo, S.-Y., Kim, J.-H., Min, C.-O., Han, D.-I., and Cho, S.-J., "Development of an Electro-optical System for Small UAV," *Aerospace Science and Technology*, Vol. 14, No. 7, Oct 2010, pp. 505–511.

[25] Kochenderfer, M. J., Edwards, M. W. M., Espindle, L. P., Kuchar, J. K., and Griffith, J. D., "Airspace Encounter Models for Estimating Collision Risk," *AIAA Journal of Guidance, Control, and Dynamics*, Vol. 33, No. 2, Mar 2010, pp. 487–499.

[26] Chryssanthacopoulos, J. P. and Kochenderfer, M. J., "Accounting for State Uncertainty in Collision Avoidance," *AIAA Journal of Guidance, Control, and Dynamics*, Vol. 34, No. 4, Jul 2011, pp. 951–960.

[27] Billingsley, T. B., Kochenderfer, M. J., and Chryssanthacopoulos, J. P., "Collision Avoidance for General Aviation," *IEEE Aerospace and Electronic Systems Magazine*, Vol. 27, No. 7, Jul 2012, pp. 4–12.

[28] Heisey, C. W., Hendrickson, A. G., Chludzinski, B. J., Cole, R. E., Ford, M., Herbek, L., Ljungberg, M., Magdum, Z., Marquis, D., Mezhirov, A., Pennell, J. L., Roe, T. A., and Weinert, A. J., "A Reference Software Architecture to Support Unmanned Aircraft Integration in the National Airspace System," *Journal of Intelligent & Robotic Systems*, Vol. 69, No. 1-4, Jan 2013, pp. 41–55.

[29] Lee, H.-T., Meyn, L. A., and Kim, S., "Probabilistic Safety Assessment of Unmanned Aerial System Operations," *AIAA Journal of Guidance, Control, and Dynamics*, Vol. 36, No. 2, Mar 2013, pp. 610–616.

[30] Owen, M. P., Duffy, S. M., and Edwards, M. W. M., "Unmanned Aircraft Sense and Avoid Radar: Surrogate Flight Testing Performance Evaluation," *IEEE Radar Conference*, Cincinnati, OH, May 2014, pp. 548–551.

[31] Edwards, M. W. M. and Owen, M. P., "Validating a Concept for Airborne Sense and Avoid," *American Control Conference*, Portland, OR, Jun 2014, pp. 1192–1197.

[32] International Civil Aviation Organization, *International Standards and Recommended Practices, Annex 10*, Vol. I: Radio Navigation Aids, New Zealand, sixth ed., July 2006.

[33] RTCA SC-159, "Minimum Operational Performance Standards for GPS Local Area Augmentation System Airborne Equipment," Dec 2008.

[34] RTCA SC-159, "Minimum Operational Performance Standards for GPS Ground-Based Regional Augmentation System Airborne Equipment," Mar 2008.

[35] RTCA SC-159, "Minimum Operational Performance Standards for Global Positioning System / Aircraft-Based Regional Augmentation System Airborne Equipment," Apr 2009.

[36] Federal Aviation Administration, "Global Positioning System Wide Area Augmentation System Performance Standard, First Edition," Oct 2008.

[37] RTCA SC-159, "Minimum Operational Performance Standards for Global Positioning System/Satellite-Based Augmentation System Airborne Equipment Change 1," Feb 2013.

[38] RTCA SC-186, "Minimum Aviation System Performance Standards for Automatic Dependent Surveillance - Broadcast (ADS-B) Change 1," Dec 2006.

[39] RTCA SC-186, "Minimum Aviation System Performance Standards for Aircraft Surveillance Applications Change 1," Dec 2006.

[40] RTCA SC-186, "Minimum Aviation System Performance Standards for ADS-B Traffic Surveillance Systems and Applications (ATSSA)," Jun 2012.

[41] Kelly, R. J. and Davis, J. M., "Required Navigation Performance (RNP) for Precision Approach and Landing with GNSS Application," *Navigation, Journal of the Institute of Navigation*, Vol. 41, No. 1, Spring 1994, pp. 1–30.

[42] Pullen, S., "What are the Differences Between Accuracy, Integrity, Continuity, and Availability, and How are they Computed?" *InsideGNSS*, Sep-Oct 2008, pp. 20–24.

[43] Jamoom, M. B., *Unmanned Aircraft System Sense and Avoid Integrity and Continuity*, Ph.D. thesis, Illinois Institute of Technology, May 2016.

[44] Gelb, A., editor, *Applied Optimal Estimation*, The MIT Press, sixteenth ed., 2001.

[45] Smearcheck, S., Calhoun, S., Adams, W., Kresge, J., and Kunzi, F., "Analysis of Alerting Performance for Detect and Avoid of Unmanned Aircraft Systems," *IEEE/ION PLANS*, Savannah, GA, Apr 2016, pp. 710–730.

[46] Kunzi, F., *Development of a High-Precision ADS-B Based Conflict Alerting System for Operations in the Airport Environment*, Ph.D. thesis, Massachusetts Institute of Technology, Oct 2013.

[47] Federal Aviation Administration, "Sense and Avoid (SAA) for Unmanned Aircraft Systems (UAS), SAA Workshop Final Report," Oct 2009.

[48] Skidmore, T. A., van Graas, F., and Liu, F., "Ohio University LAAS Monitoring: Design and Performance," *Proceedings of the 9th International Technical Meeting of the Satellite Division of The Institute of Navigation (ION GPS 1996)*, Kansas City, MO, Sep 1996, pp. 1615–1621.

[49] Enge, P., "Local Area Augmentation of GPS for the Precision Approach of Aircraft," *Proceedings of the IEEE*, Vol. 87, No. 1, Jan 1999, pp. 111–132.

[50] Lee, Y. C., "Analysis of Range and Position Comparison Methods as a Means to Provide GPS Integrity in the User Receiver," *Proceedings of the 42nd Annual Meeting of The Institute of Navigation*, Seattle, WA, Jun 1986, pp. 1–4.

[51] Parkinson, B. W. and Axelrad, P., "Autonomous GPS Integrity Monitoring Using the Pseudorange Residual," *Navigation, Journal of The Institute of Navigation*, Vol. 35, No. 2, Summer 1988, pp. 255–274.

[52] Pervan, B. S., Pullen, S. P., and Christie, J. R., "A Multiple Hypothesis Approach to Satellite Navigation Integrity," *Navigation, Journal of The Institute of Navigation*, Vol. 45, No. 1, Spring 1998, pp. 62–71.

[53] Kochenderfer, M. J., Kuchar, J. K., Espindle, L. P., and Griffith, J. D., "Uncorrelated Encounter Model of the National Airspace System," Project Report ATC-345, Massachusetts Institute of Technology, Lincoln Laboratory, 2008.

[54] Weinert, A., Harkleroad, E., Griffith, J., Edwards, M., and Kochenderfer, M., "Uncorrelated Encounter Model of the National Airspace System Version 2.0," Project Report ATC-404, Massachusetts Institute of Technology, Lincoln Laboratory, 2013.

[55] RTCA SC-147, "Minimum Operational Performance Standards for Traffic Alert and Collision Avoidance System II," 2008.

[56] Chen, R. H., Gevorkian, A., Fung, A., Chen, W.-Z., and Raska, V., "Multi-Sensor Data Integration for Autonomous Sense and Avoid," *AIAA Infotech@Aerospace*, St Louis, MO, Mar 2011.

[57] RTCA SC-228, "Draft Minimum Operational Performance Standards for for Air-to-Air Radar for Detect and Avoid Systems," Apr 2016.

[58] Edwards, M., "A Safety Driven Approach to the Development of an Airborne Sense and Avoid System," *Infotech@Aerospace 2012*, American Institute of Aeronautics and Astronautics (AIAA), Garden Grove, CA, Jun 2012, pp. 1–12.

[59] Federal Aviation Administration, "Advisory Circular 25.1309-1A - System Design and Analysis," Jun 1988.

[60] Griffith, J., Owen, M., and Weinert, A., "An Approach to Develop Surveillance Accuracy Requirements for Sense and Avoid," Project Report ATC-407, Massachusetts Institute of Technology, Lincoln Laboratory, 2013.

[61] DeCleene, B., "Defining Pseudorange Integrity - Overbounding," *Institute of Navigation GPS Conference*, Salt Lake City, UT, Sep 2000, pp. 1916–1924.

[62] Rife, J., Pullen, S., Enge, P., and Pervan, B., "Paired Overbounding for Nonideal LAAS and WAAS Error Distributions," *IEEE Transactions on Aerospace and Electronic Systems*, Vol. 42, No. 4, Oct 2006, pp. 1386–1395.